

Universal Scaling and Signatures of Nodal Structures in Electron Tunneling from Two-Dimensional Semimetals

Yee Sin Ang,^{1,*} Ching Hua Lee,^{2,3,†} and L. K. Ang^{1,‡}

¹*Science and Math, Singapore University of Technology and Design, Singapore 487372*

²*Department of Physics, National University of Singapore, Singapore 117542*

³*Institute of High Performance Computing, A*STAR, Singapore 138632*

We present the theory of out-of-plane electron thermal-field emission from 2D semimetals. We show that the current(\mathcal{J})-field(F)-temperature(T) characteristic is captured by a *universal* scaling law applicable for broad classes of 2D semimetals, including monolayer and few-layer graphene, nodal point semimetals, nodal line semimetals and Dirac semimetals at the verge of topological phase transition. The low-temperature scaling takes the universal form, $\log(\mathcal{J}/F^\gamma) \propto -1/F$ with $\gamma = 1$ for 2D semimetals, which is in stark contrast to the classic Fowler-Nordheim scaling of $\gamma = 2$ for 3D metals. Importantly, the Fermi level dependence of the tunneling currents depends sensitively on the nodal structure through the electronic density of states, thus serving as a probe for detecting the various possible nodal structures of 2D semimetals. Our findings provide a theoretical basis for the understanding of tunneling charge transport phenomena in solid/vacuum and solid/solid interfaces, critical for the development of 2D-material-based vacuum and solid-state electronic devices.

Introduction.— In two-dimensional (2D) materials, the confinement of electrons within atomic-scale thickness and the emergence of fermions with exotic dispersions lead to unusual transport properties unique to 2D [1, 2] such as Klein tunneling [3], unconventional quantum Hall [4] and spin Hall effects [5], valley contrasting transport [6] and spontaneous berryogenesis [7]. Particularly in thermionic emission, where electrons are emitted from a surface via semiclassical thermal excitation, the universal current-temperature scaling law represents another fascinating transport manifestation of the reduced dimensionality of 2D materials [8], challenging the century-old Richardson-Dushman thermionic emission theory [9] in the 2D *Flatland*.

Apart from thermionic emission, electron can undergo quantum mechanical *field emission* [10] when an external applied field strongly enhances the electron tunneling from a solid surface by “narrowing” the interface potential barrier. Fowler-Nordheim (FN) theory [11] has been the key theoretical foundation for electron field emission in bulk (3D) materials, and stood as a central pillar of vacuum device technology. Remarkably, field emission physics remains highly important to solid-state devices today due to its critical role in interfacial charge injection processes across the metal/insulator and metal/semiconductor interfaces [12], which are omnipresent in modern electronic and optoelectronic devices. Due to its technological importance in both vacuum [13] and solid-state device technology, FN theory has been continually refined over the past decades [14–18].

In 2D materials, the validity of FN-type theories need to be scrutinized since their fundamental assumption of 3D parabolic dispersions are fundamentally incompatible with 2D materials [19]. Despite ongoing experimental [20–30] and theoretical [31–34] efforts in unearthing the physics of electron emission from graphene, a comprehensive understanding of electron emission from the

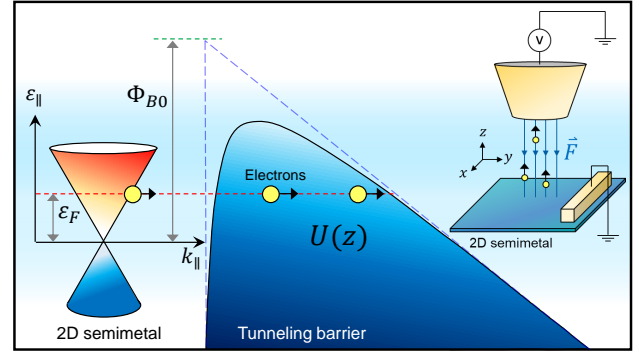


FIG. 1. Sketch of energy barrier in electron emission from 2D semimetals. $U(z)$ is the interface potential barrier inclusive of the image charge. Inset: Schematic drawing of electron emission measurement under an applied electric field F .

broader family of 2D semimetals remains largely incomplete. The following questions remain open: (i) How does the field emission current relate to the applied electric field strength and emitter temperature? (ii) What are radical differences between the electron field emission in 2D and 3D materials? (iii) Is there a unifying scaling relation, counterpart to the universal current-temperature scaling law of semiclassical thermionic emission [8], that encompasses field emission characteristics for generic 2D semimetals? (iv) Can emission characteristics reveal the nature of nodal structures of 2D semimetals?

In this work, we address the above questions by developing the theory of out-of-plane electron thermal-field emission from 2D semimetals. We present full numerical and approximate analytical expressions of the thermal-field emission current [14] for various 2D semimetals, including monolayer and few-layer graphene[1], nodal point semimetals [35] of generalized pseudospin vorticity [36], Dirac semimetals at the verge of topological phase transi-

tion [37] and nodal line semimetals [38]. Remarkably, by employing a generalized model of 2D semimetals [8], we show that the emission current density (\mathcal{J}_{2D}) for broad classes of 2D semimetals can be captured by a *universal* current-field-temperature scaling law,

$$\mathcal{J}_{2D}(F, T) \approx \mathcal{A} \frac{\pi d_F}{c \sin(\pi/c)} \exp\left(-\frac{\mathcal{B}}{F}\right), \quad (1)$$

where \mathcal{A} and \mathcal{B} are material-dependent parameters, F is the electric field strength, T is the emitter temperature, $d_F \propto F$ is a field-dependent parameter (defined below), and $c \equiv d_F/k_B T$. In particular, Eq. (1) departs from the 3D material thermal-field emission scaling law $\mathcal{J}_{3D} = \mathcal{A}\pi d_F^2/c \sin(\pi/c) \exp(-\mathcal{B}/F)$ [14], thus revealing the fundamental incompatibility of classic FN-type theories with 2D semimetals.

The universal thermal-field emission scaling law identified here reveals an important feature of thermal-field emission in 2D: It is fundamentally determined by the *density of states* and dispersion profile of the 2D material, and hence exhibits strong *Fermi level dependence*. In particular, it is the topology of nodal structure, *not* band topology, that corresponds to markedly distinct transport regimes, as presented in Fig. 2. This contrasts with various other electronic, optical, electrical, mechanical and thermodynamical properties, where signatures of nontrivial *band* topology are also manifested in the density of states [39], transport [40, 41], optical response [42–44], quantum oscillations [46, 89], many-body behavior [48–50], and shear viscosity [36]. As electron field emission is a key charge transport mechanism in both solid/vacuum [51] and solid/solid interfaces [54, 55], the model developed here shall offer a pivotal theoretical foundation for both the fundamental understanding of nanoscale surface physics, and the design of novel vacuum [52] and solid-state devices based on 2D materials heterostructures [53].

2D electron emission theory.— In a 2D system, the confinement of electrons within the 2D plane lead to the formation of discrete subbands. The energy dispersion and the wavevector of the i th-subband are, $\varepsilon_{\mathbf{k}_i} = \varepsilon_{\parallel,i}(\mathbf{k}_{\parallel,i}) + \varepsilon_{\perp,i}(\mathbf{k}_{\perp,i})$ and $\mathbf{k}_i = \mathbf{k}_{\parallel,i} + \mathbf{k}_{\perp,i}$, respectively, where $\varepsilon_{\perp,i}$ and $\mathbf{k}_{\perp,i}$ denotes the discrete subband energy and the quantized wavevector along the out-of-plane direction, respectively; $\varepsilon_{\parallel,i}$ and $\mathbf{k}_{\parallel,i}$ denotes the continuously-dispersing *in-plane* energy dispersion and wavevector, respectively. The out-of-plane electron emission current density can be generally expressed as [36]:

$$\mathcal{J}_{2D}(F, T) = \frac{ge}{(2\pi)^2} \sum_i \tau_{\perp,i}^{-1} \int_{\text{B.Z.}} d^2\mathbf{k}_{\parallel,i} D(\mathbf{k}_i, F) f(\mathbf{k}_i, \mathbf{k}_F), \quad (2)$$

where g is the degeneracy factor, \mathbf{k}_F is the Fermi wavevector, $D(\mathbf{k})$ is the *out-of-plane* tunneling probability, $f(\mathbf{k}_i)$ is the Fermi-Dirac distribution function, the \mathbf{k}_{\parallel} -integral spans the whole Brillouin zone, \sum_i runs over

all subbands, and τ_{\perp}^{-1} is the vertical electron injection rate, which is affected by the intrinsic material properties and the device configuration, and can be experimentally extracted from the transport measurements [69–71]. The transmission probability, $D(\mathbf{k}_i, F)$, is a function of the *total* wavevector, \mathbf{k}_i , instead of only the out-of-plane component $\mathbf{k}_{\perp,i}$, due to the $\mathbf{k}_{\parallel,i}$ -nonconserving scatterings [56–62], which can arise extrinsically from electron-electron [56], phonon [63], magnon [64], and defects [57, 65] scatterings. Such momentum nonconservation leads to the coupling of the $\mathbf{k}_{\perp,i}$ and $\mathbf{k}_{\parallel,i}$ during the out-of-plane tunneling process [8].

For thermal-field emission, the tunneling potential barrier is modeled, with inclusion of the image-charge effect across a dielectric interface, as $U(z) = \Phi_{B0} - eFz - e^2\nu/16\pi\epsilon_0 z$, where Φ_{B0} is the *intrinsic* interface potential barrier height measured from zero-energy, $\nu \equiv (\epsilon_s - 1)/(\epsilon_s + 1)$, and ϵ_s is the dielectric constant of the substrate material (see Fig. 1). The corresponding transmission probability can be accurately approximated as [14], $D(\mathbf{k}_i, F) \approx D_F \exp\{[\varepsilon_{\parallel}(\mathbf{k}_{\parallel,i}) + \varepsilon_{\perp,i}(\mathbf{k}_{\perp,i}) - \varepsilon_F]/d_F\}$, where $d_F \equiv \hbar eF/(8m_0)^{1/2} (\Phi_{B0} - \varepsilon_F)^{1/2} t_0$, $D_F \equiv \exp[-4(2m_0)^{1/2} (\Phi_{B0} - \varepsilon_F)^{3/2} v_0/3\hbar eF]$, v_0 and t_0 correction factors for the image charge effect, and m_0 is the free electron mass (see [66] for detailed derivations). Considering the typical case where there is only one subband around the Fermi level ε_F , Eq. (2) becomes

$$\mathcal{J}_{2D}(F, T) = \frac{geD_F}{4\pi^2\tau_{\perp}} \int_{\text{B.Z.}} d^2\mathbf{k}_{\parallel} \frac{\exp\left(\frac{\varepsilon_{\parallel} - \varepsilon_F}{d_F}\right)}{\exp\left(\frac{\varepsilon_{\parallel} - \varepsilon_F}{k_B T}\right) + 1}, \quad (3)$$

where k_{\parallel} and ε_{\parallel} denote the in-plane wavevector and energy components of the subband undergoing emission.

We now express the emission current in Eq. (3) in terms of a 2D anisotropic density of states (DOS). The DOS is defined as $\rho(\varepsilon_{\parallel})d\varepsilon_{\parallel} = [g/(2\pi)^2] \int_0^{2\pi} d\phi k_{\parallel} dk_{\parallel}$ where $k_{\parallel} \equiv |\mathbf{k}_{\parallel}|$. Very generally, we can express the k_{\parallel} -differential as a two-variable polynomial, i.e. $k_{\parallel} dk_{\parallel} = \sum_{m,l=0}^{\infty} \beta_{ml} |\varepsilon_{\parallel}|^m \cos^l \phi d\varepsilon_{\parallel}$ where β_{ml} is an expansion coefficient of (m, l) -order in $(\varepsilon_{\parallel}, \cos \phi)$, which yields

$$\rho(\varepsilon_{\parallel}) = g \sum_{m=0}^{\infty} \bar{\beta}_m |\varepsilon_{\parallel}|^m, \quad (4)$$

where $m \in \mathbb{Z}^{\geq 0}$ and $\bar{\beta}_m$ is defined as [66],

$$\begin{aligned} \bar{\beta}_m &= \sum_l \frac{\beta_{ml}}{(2\pi)^2} \int_0^{2\pi} \cos^l \phi d\phi \\ &= \frac{\beta_{m0}}{2\pi} + \sum_{l \in \text{even}, > 0} \frac{\beta_{ml}}{2\pi} \prod_{k=1}^l \frac{2k-1}{2k} \end{aligned} \quad (5)$$

Combining Eqs. (3) and (4), the *universal* thermal-field emission electrical current density from a 2D semimetal

becomes $\mathcal{J}_{\text{uni}} = \sum_m^\infty \mathcal{J}_{\text{uni}}^{(m)}$ where the m -component is,

$$\mathcal{J}_{\text{uni}}^{(m)} = \frac{geD_F}{\tau_\perp} \bar{\beta}_m \int_{-\infty}^{\Phi_{B0}} d\varepsilon_\parallel |\varepsilon_\parallel|^m \frac{\exp\left(\frac{\varepsilon_\parallel - \varepsilon_F}{d_F}\right)}{\exp\left(\frac{\varepsilon_\parallel - \varepsilon_F}{k_B T}\right) + 1}, \quad (6)$$

which cannot be analytically solved except for the case of $m = 0$. An approximate *analytical* expression can be obtained by making the following *ansatz*. The term $|\varepsilon_\parallel|^m$ is replaced by $\xi_m |\varepsilon_F|^m$ since field emission is dominantly contributed by electrons residing around ε_F . Here ξ_m is a correction factor for the m -th order term which can be obtained by fitting the full numerical results with the analytical approximation derived below. By a substitution $u = \exp[(\varepsilon_\parallel - \varepsilon_F)/d_F]$, Eq. (6) becomes [66]

$$\mathcal{J}_{\text{uni}}^{(m)} \approx \xi_m \frac{geD_F}{\tau_\perp} \bar{\beta}_m |\varepsilon_F|^m d_F \int_0^\infty \frac{du}{u^c + 1}, \quad (7)$$

where $c \equiv d_F/k_B T$. The above integral can be analytically evaluated [14] for the thermal-field emission condition of $c > 1$ (i.e. $d_F > k_B T$ which remains valid for $T \lesssim 550$ K at $F = 1$ V/nm),

$$\mathcal{J}_{\text{uni}} \approx \xi_m \frac{ge}{\tau_\perp} \sum_{m=0}^\infty \bar{\beta}_m |\varepsilon_F|^m \frac{\pi d_F}{c \sin(\pi/c)} D_F. \quad (8)$$

We evaluate the full numerical solution [Eq. (6)] and the analytical approximation [Eq. (8)] for $m = 0, 1, 2, 3, 4$ (Fig. 2). The approximate solution agrees well with the full numerical results over the range of $F = 1$ V/nm to $F = 5$ V/nm with $\xi_m = (1, 1.22, 4, 24, 220)$ for $m = 0$ to $m = 4$. From Eq. (8), we obtain the following scaling law,

$$\mathcal{J} \propto \frac{\pi d_F}{c \sin(\pi/c)} D_F. \quad (9)$$

Equation (9) represents a *universal* current-field-temperature scaling law for 2D semimetals as long as the DOS near ε_F can be captured by the anisotropic DOS model in Eq. (4). Equation (9) thus offer a simple unifying scaling law description of the thermal-field emission characteristics in 2D semimetals. Below, we derive the thermal-field emission characteristics for several representative 2D semimetals, including: (i) graphene and its few-layer; (ii) nodal point semimetal; (iii) Dirac semimetal near topological phase transition; and (iv) nodal line semimetal, and show that their current-field-temperature scaling relation universally converges to Eq. (9) (summarized in Fig. 2).

Graphene.— We first consider graphene, a 2D Dirac semimetal, which can be described by the effective Hamiltonian, $\mathcal{H}_{\text{Gr}}(\mathbf{k}_\parallel) = \hbar v_F (k_x \sigma_x + k_y \sigma_y)$ where $\mathbf{k}_\parallel = (k_x, k_y)$ is the in-plane wavevector, $\sigma_{x,y}$ is the Pauli matrices, and $v_F = 10^6$ m/s. Using the procedure described

above, the thermal-field emission current density can be solved as,

$$\mathcal{J}_{\text{Gr}}/\psi \approx \frac{2e\Phi_{B0}}{\tau_\perp \pi \hbar^2 v_F^2} \left(\frac{|\varepsilon_F|}{\Phi_{B0}}\right)^{1+\eta} \frac{\pi d_F}{c \sin(\pi/c)} D_F. \quad (10)$$

where ε_F (also implicit in d_F , c and D_F) is a function of the applied electric field strength, i.e. $\varepsilon_F = \varepsilon_F(F)$, due to the field-effect tunable Fermi level in graphene [72]. Assuming a planar geometry and an undoped graphene with $\varepsilon_F(F=0) = 0$, we obtain [66] $\varepsilon_F(F) = \sqrt{\pi \hbar^2 v_F^2 \varepsilon_0 F/e}$ with $\eta = 0.176$ as fitted from the full numerical solution. Apart from exhibiting the universal scaling, \mathcal{J}_{2D} follows the ε_F -dependence, $\mathcal{J}_{\text{Gr}}/\psi \propto |\varepsilon_F|^{1+\eta}$ where $\psi \equiv \pi d_F D_F / c \sin(\pi/c)$. As demonstrated below, the \mathcal{J}/ψ - ε_F scaling is sensitively influenced by the nodal structure, thus serving as a tool to probe different possible nodal structures of 2D semimetals (see Table I).

Nodal point semimetal.— We next consider a general model of 2D nodal point semimetal with the effective Hamiltonian [36],

$$\hat{\mathcal{H}}_{\text{NP}}(\mathbf{k}_\parallel) = \alpha_n (k_x^n \sigma_x + k_y^n \sigma_y), \quad (11)$$

where α_n is a material-dependent parameter, and $n \in \mathbb{Z}^+$ denotes the pseudospin vorticity. Equation (11) also describes the low-energy quasiparticles in n -layer graphene of Bernal stacking configuration with $\alpha_n = (\hbar v_F)^n / t_\perp^{n-1}$ and $t_\perp = 0.39$ eV [1]. The thermal-field emission current density is,

$$\mathcal{J}_{\text{NP}} \approx \xi_n \frac{ge}{2\pi\tau_\perp} \frac{|\varepsilon_F|^{2/n-1}}{n\alpha_n^{2/n}} \frac{\pi d_F}{c \sin(\pi/c)} D_F. \quad (12)$$

Here the emission current density follows a particularly interesting ε_F -scaling of $\mathcal{J}_{\text{NP}}/\psi \propto |\varepsilon_F|^{2/n-1}$ which depends on the pseudospin vorticity, n .

Dirac semimetal near criticality.— We now consider a 2D Dirac semimetal near criticality, such as black phosphorus monolayer subjected to a strong vertical electric field [67]. Such system is captured by the effective *semi-Dirac* Hamiltonian,

$$\hat{\mathcal{H}}_{\text{SD}}(\mathbf{k}_\parallel) = \hbar v_x k_x \sigma_x + (b k_y^2 + \Delta) \sigma_y, \quad (13)$$

where v_x and b are band structure parameters. The system undergoes a critical phase transition when Δ is switched from $\Delta \leq 0$ to $\Delta > 0$, with two Dirac cones merging into one at $\Delta = 0$ and then gapping out. In the semimetallic phase ($\Delta \leq 0$), the thermal-field emission current density is

$$\mathcal{J}_{\text{SD}} \approx \xi \frac{ge|\varepsilon_F|}{(2\pi)^2 \tau_\perp b} \mathcal{I}_{\phi, \varepsilon_F}(\Delta/\varepsilon_0) \frac{\pi d_F}{c \sin(\pi/c)} D_F \quad (14)$$

where $\varepsilon_0 \equiv \hbar^2 v_F^2 / b$ is a characteristic energy scale and $\phi = \tan^{-1}(k_y/k_x)$. The ϕ -integral $\mathcal{I}_{\phi, \varepsilon_F}(\mu) \equiv \int_0^{2\pi} d\phi [\Lambda_{\phi, \mu} - 4 \sin^2 \phi (\mu^2 - \varepsilon_F^2/\varepsilon_0^2)]^{1/2}$, where $\Lambda_{\phi, \mu} \equiv$

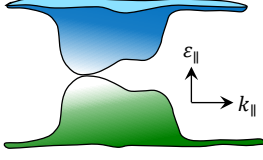
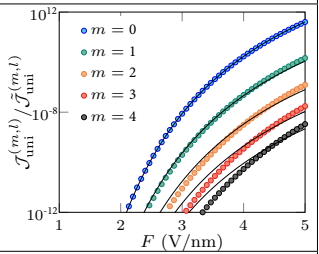
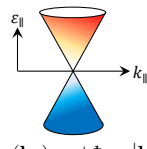
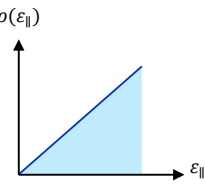
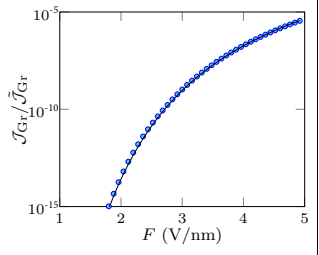
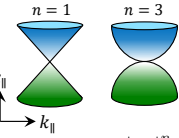
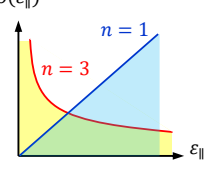
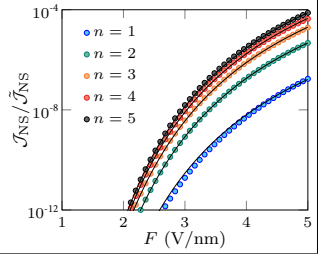
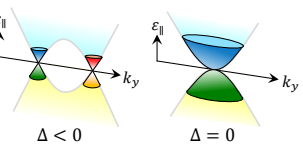
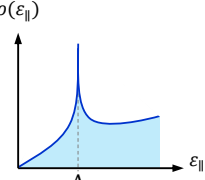
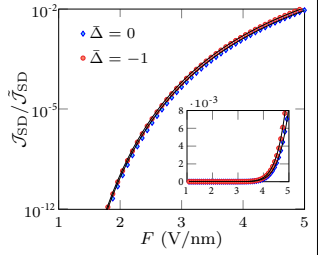
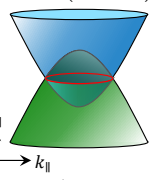
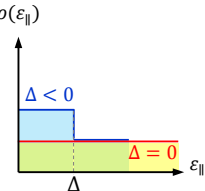
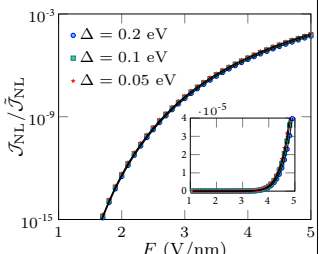
2D system	Density of states	Thermal-field emission current density	Numerical vs. approximation
Generalized 2D anisotropic band 	$\rho(\varepsilon_{\parallel}) = g \sum_{m=0}^{\infty} \bar{\beta}_m \varepsilon_{\parallel} ^m$	$\frac{\mathcal{J}_{\text{uni}}^{(m)}}{\tilde{\mathcal{J}}_{\text{uni}}^{(m)}} = D_F \int_{-\infty}^{\Phi_{B0}} \bar{\varepsilon}_{\parallel} ^m \mathcal{G}_{\text{TF}}(\bar{\varepsilon}_{\parallel}, \bar{d}_F, \bar{T}) d\bar{\varepsilon}_{\parallel}$ $\mathcal{J}_{\text{uni}}^{(m)} \approx \xi_m \frac{ge}{\tau_{\perp}} \bar{\beta}_m \varepsilon_F ^m \frac{\pi d_F}{c \sin(\pi/c)} D_F$	
Graphene monolayer $\mathcal{H}_{\text{Gr}}(\mathbf{k}_{\parallel}) = \hbar v_F (k_x \sigma_x + k_y \sigma_y)$  $\varepsilon_{\parallel}(\mathbf{k}_{\parallel}) = \pm \hbar v_F \mathbf{k}_{\parallel} $		$\frac{\mathcal{J}_{\text{Gr}}}{\tilde{\mathcal{J}}_{\text{Gr}}} = D_F \int_{-\infty}^{\Phi_{B0}} \bar{\varepsilon}_{\parallel} \mathcal{G}_{\text{TF}}(\bar{\varepsilon}_{\parallel}, \bar{d}_F, \bar{T}) d\bar{\varepsilon}_{\parallel}$ $\mathcal{J}_{\text{Gr}} \approx \frac{2e\Phi_{B0}}{\tau_{\perp} \pi \hbar^2 v_F^2} \left(\frac{ \varepsilon_F }{\Phi_{B0}} \right)^{1+\eta} \frac{\pi d_F}{c \sin(\pi/c)} D_F$	
Nodal point semimetal $\mathcal{H}_{\text{NP}}(\mathbf{k}_{\parallel}) = \alpha_n (k_x^n \sigma_x + k_y^n \sigma_y)$  $\varepsilon_{\parallel}(\mathbf{k}_{\parallel}) = \pm \alpha_n \mathbf{k}_{\parallel} ^n$		$\frac{\mathcal{J}_{\text{NP}}}{\tilde{\mathcal{J}}_{\text{NP}}} = D_F \int_{-\infty}^{\Phi_{B0}} \bar{\varepsilon}_{\parallel} ^{2/n-1} \mathcal{G}_{\text{TF}}(\bar{\varepsilon}_{\parallel}, \bar{d}_F, \bar{T}) d\bar{\varepsilon}_{\parallel}$ $\mathcal{J}_{\text{NP}} \approx \xi_n \frac{ge}{2\pi\tau_{\perp}} \frac{ \varepsilon_F ^{2/n-1}}{n\alpha_n^{2/n}} \frac{\pi d_F}{c \sin(\pi/c)} D_F$	
Dirac semimetal near criticality $\mathcal{H}_{\text{SD}}(\mathbf{k}_{\parallel}) = \hbar v_x k_x \sigma_x + (b k_y + \Delta)^2 \sigma_y$  $\varepsilon_{\parallel}(\mathbf{k}_{\parallel}) = \pm \sqrt{\hbar^2 v_x^2 k_x^2 + (b k_y + \Delta)^2}$		$\frac{\mathcal{J}_{\text{SD}}}{\tilde{\mathcal{J}}_{\text{SD}}} = D_F \int_0^{2\pi} d\phi$ $\times \left(\int_{-\infty}^{-\frac{\Phi_{B0}}{\varepsilon_0}} + \int_{-\tilde{\Delta}}^{\tilde{\Delta}} \right) \frac{ \bar{\varepsilon}_{\parallel} \mathcal{G}_{\text{TF}}(\bar{\varepsilon}_{\parallel}, \bar{d}_F, \bar{T}) d\bar{\varepsilon}_{\parallel}}{\sqrt{\Lambda_{\phi, \tilde{\Delta}} - 4 \sin^4 \phi (\tilde{\Delta}^2 - \bar{\varepsilon}_{\parallel}^2)}}$ $\mathcal{J}_{\text{SD}} \approx \xi \frac{ge \varepsilon_F }{(2\pi)^2 \tau_{\perp} b} \mathcal{I}_{\phi}(\Delta/\varepsilon_0) \frac{\pi d_F}{c \sin(\pi/c)} D_F$	
Nodal line semimetal $\mathcal{H}_{\text{NL}}(\mathbf{k}_{\parallel}) = (b k_{\parallel}^2 - \Delta) \sigma_x$  $\varepsilon_{\parallel}(\mathbf{k}) = \pm b \mathbf{k}_{\parallel} ^2 - \Delta $		$\frac{\mathcal{J}_{\text{NL}}}{\tilde{\mathcal{J}}_{\text{NL}}} = D_F \left(\int_{-\infty}^{-\tilde{\Delta}} + \int_{-\tilde{\Delta}}^{\tilde{\Delta}} \right) \mathcal{G}_{\text{TF}}(\bar{\varepsilon}_{\parallel}, \bar{d}_F, \bar{T}) d\bar{\varepsilon}_{\parallel}$ $\mathcal{J}_{\text{NL}} \approx \xi \frac{ge}{4\pi b \tau_{\perp}} \frac{\pi d_F}{c \sin(\pi/c)} D_F$	

FIG. 2. Thermal-field electron emission from 2D semimetals, showing energy dispersion (column 1), density of states (column 2), numerical and approximate expressions of the thermal-field emission current density (column 3), and the normalized current (column 4) evaluated at $T = 300$ K, $\epsilon_s = 3.5$, and $\Phi_{B0} = 4.5$ eV. For nodal semimetal, Dirac semimetal near criticality and nodal line semimetal, $\varepsilon_F = 0.1$ eV is used. The full numerical and the analytical approximate solutions are denoted by circle and solid curves, respectively. The normalized currents are defined as: $\tilde{J}_{\text{NP}} = ge\Phi_{B0}^2/2\pi n\tau_{\perp}\alpha_n^{2/n}$, $\tilde{J}_{\text{QCP}} = \xi ge\varepsilon_F\Phi_{B0}\mathcal{I}_{\phi, \varepsilon_F}(\Delta/\varepsilon_0)/4\pi^2\tau_{\perp}b$, $\tilde{J}_{\text{Gr}} = 2e\Phi_{B0}^2/\pi\hbar^2v_F^2\tau_{\perp}$ and $\tilde{J}_{\text{uni}} = ge\tau_{\perp}^{-1}\sum_{m=0}^{\infty}\bar{\beta}_m$. Here, $\bar{\varepsilon}_{\parallel} \equiv \varepsilon_{\parallel}/\Phi_{B0}$, $\bar{d}_F \equiv d_F/\Phi_{B0}$, $\bar{T} \equiv k_B T/\Phi_{B0}$, $\tilde{\varepsilon}_{\parallel} \equiv \varepsilon_{\parallel}/\Phi_{B0}$, $\tilde{d}_F \equiv d_F/\Phi_{B0}$, $\tilde{T} \equiv k_B T/\Phi_{B0}$, $\tilde{\Delta} \equiv \Delta/\varepsilon_0$, and $\mathcal{G}_{\text{TF}}(\varepsilon_F, d_F, T) \equiv e^{(\varepsilon_{\parallel} - \varepsilon_F)/d_F} / (e^{(\varepsilon_{\parallel} - \varepsilon_F)/k_B T} + 1)$. The correction factors are $\eta = 0.176$ for graphene, and the ξ 's of other 2D semimetals are outlined in the Supplemental Material [66].

TABLE I. The current versus Fermi level scaling relation for various 2D semimetals.

2D System	ε_F dependence of \mathcal{J}/ψ
Graphene	$ \varepsilon_F ^{1+\eta}$
Nodal point semimetal	$ \varepsilon_F ^{2/n-1}$
Dirac semimetal near criticality	$ \varepsilon_F \mathcal{I}_{\phi, \varepsilon_F}(\Delta/\varepsilon_0)$
Nodal line semimetal	constant in ε_F

$(\cos^2 \phi + 2\mu \sin^2 \phi)^2$, arises from the broken rotational symmetry of Eq. (13). In this case, $\mathcal{J}_{SD}/\psi \propto |\varepsilon_F| \mathcal{I}_{\phi, \varepsilon_F}(\Delta/\varepsilon_0)$.

Nodal line semimetal.— In a 2D nodal line semimetal, the band touching of two bands extends from a discrete nodal point into a continuous one-dimensional open nodal line or closed nodal ring in phase space. We consider a representative 2D semimetal that hosts an isotropic iso-energy nodal loop, such as carbon nitride monolayer [68], as described by,

$$\mathcal{H}_{NL}(\mathbf{k}_{\parallel}) = (bk_{\parallel}^2 - \Delta) \sigma_x \quad (15)$$

where Δ is a band inversion parameter. Solving Eq. (3) yields the approximate solution,

$$\mathcal{J}_{NL} \approx \xi \frac{ge}{4\pi b\tau_{\perp}} \frac{\pi d_F}{c \sin(\pi/c)} D_F, \quad (16)$$

where \mathcal{J}_{NL}/ψ is constant in ε_F .

Before closing this work, we make four remarks. Firstly, in the ‘cold’ field emission regime ($T \rightarrow 0$), Eq. (9) becomes $\mathcal{J}_{2D}(F, T \rightarrow 0) \propto d_F D_F$, which is in stark contrast to the FN law for bulk materials, $\mathcal{J}_{3D}(F, T \rightarrow 0) \propto d_F^2 D_F$. Ignoring the image-charge effect, the *FN plot* [73] widely used in characterizing electron field emission and solid-state tunneling charge injection can thus be generalized as,

$$\log\left(\frac{\mathcal{J}}{F^{\gamma}}\right) \propto -\frac{1}{F}, \quad (17)$$

where $\gamma = 1$ and 2 , respectively, for 2D and 3D materials. Secondly, the scaling law is universal except in the case of a *non-dispersing* 2D flat bands in 2D systems such as Kagome [74], Lieb [75], α - T^3 [76], Weierstrass-function-inspired [77] and Archimedean [78] lattices. For a flat band situated at $\varepsilon_{\parallel} = \varepsilon_{FB}$, the thermal-field emission current densities is

$$\mathcal{J}_{FB} \propto D_F \frac{\exp\left(\frac{\varepsilon_{FB} - \varepsilon_F}{d_F}\right)}{1 + \exp\left(\frac{\varepsilon_{FB} - \varepsilon_F}{k_B T}\right)}, \quad (18)$$

which clearly deviates from Eq. (9). Such deviation also explains the reduced accuracy of Eq. 8 in approximating $\mathcal{J}_{uni}^{(m,l)}$ using Eq. 6 at large m since each $|\varepsilon|^{m-1}$ term

in Eq. (4) corresponds to $\varepsilon_{\parallel} \propto k_{\parallel}^{2/(m+1)}$ and thus a larger m corresponds to a ‘flatter’ dispersion. Thirdly, the thermal-field emission model developed here can be directly mapped onto the case of charge tunneling injection in the solid-state interfaces of metal/insulator and semiconductor/metal interfaces. Finally, we emphasize that although the \mathcal{J} - F - T scaling does not offer distinctive signature of nontrivial band topology, the \mathcal{J} - ε_F scaling does contain rich scaling signatures for different *nodal structures* (see Table I), which can represent cross sections of sophisticated topological structures classified by knot theory and singularity theory [79–83].

In conclusion, we developed the theory of out-of-plane thermal-field electron emission from 2D semimetals. We demonstrated the existence of a universal current-field scaling law broadly applicable for a large variety of 2D semimetals with different nodal structures. As thermal-field emission represents one of the key charge transport process across solid/vacuum and solid/solid interfaces, the universal scaling law developed here shall be a ubiquitous tool for the study and the design of vacuum electronics, nanoelectronics, optoelectronics and the emerging fields of spintronic [84], valleytronic [85] and neuromorphic [86] devices using 2D materials, and shall offer a theoretical basis for the understanding of complex electron emission phenomena, such as ultrashort-pulsed laser-induced internal photoemission [87] and photo-assisted hot carrier field emission [88, 89] in the 2D *Flatland*.

This work is supported by A*STAR-IRG (A1783C0011), and Singapore Ministry of Education (MOE) Tier 2 Grant (2018-T2-1-007).

* yeemin.ang@sutd.edu.sg

† phylch@nus.edu.sg

‡ ricky_ang@sutd.edu.sg

- [1] A. H. Castro Neto, F. Guinea, N. M. R. Peres, K. S. Novoselov, and A. K. Geim, ‘The electronic properties of graphene’, *Rev. Mod. Phys.* 81, 109 (2009).
- [2] V. K. Sangwan, and M. C. Hersam, ‘Electronic Transport in Two-Dimensional Materials’, *Annu. Rev. Phys. Chem.* 69, 299 (2018).
- [3] M. I. Katsnelson, K. S. Novoselov, and A. K. Geim, ‘Chiral tun‘nelling and the Klein paradox in graphene’, *Nat. Phys.* 2, 620 (2006).
- [4] K. S. Novoselov, E. McCann, S. V. Morozov, V. I. Fal’ko, M. I. Katsnelson, U. Zeitler, D. Jiang, F. Schedin, and A. K. Geim, ‘Unconventional quantum Hall effect and Berrys phase of 2π in bilayer graphene’, *Nat. Phys.* 2, 177 (2006).
- [5] C. L. Kane, and E. J. Mele, ‘Quantum Spin Hall Effect in Graphene’, *Phys. Rev. Lett.* 95, 226801 (2005).
- [6] D. Xiao, W. Yao, and Q. Niu, ‘Valley-Contrasting Physics in Graphene: Magnetic Moment and Topological Transport’, *Phys. Rev. Lett.* 99, 236809 (2007).
- [7] M. S. Rudner, and J. C. W. Song, ‘Self-induced Berry flux and spontaneous non-equilibrium magnetism’, *Nat.*

- Phys. 15, 1017 (2019).
- [8] Y. S. Ang, H. Y. Yang, and L. K. Ang, ‘Universal Scaling Laws in Schottky Heterostructures Based on Two-Dimensional Materials’, *Phys. Rev. Lett.* 121, 056802 (2018).
- [9] O. W. Richardson, ‘Some applications of the electron theory of matter’, *Phil. Mag.* 23, 594 (1912); S. Dushman, ‘Electron emission from metals as a function of temperature’, *Phys. Rev.* 21, 623 (1923).
- [10] K. L. Jensen, *Introduction to the Physics of Electron Emission*, Wiley (2017).
- [11] R. H. Fowler, and L. Nordheim, ‘Electron emission in intense electric fields’, *Proc. R. Soc. London Ser. A* 119, 173 (1928); W. Schottky, *Z. Phys.* 15, 872, (1923); L. W. Nordheim, *Proc. R. Soc. London, Ser. A* 121, 626 (1928).
- [12] S. M. Sze, and K. K. Ng, *Physics of Semiconductor Devices*, Wiley-Interscience, 3rd Edition (USA, 2007).
- [13] J.-W. Han, M.-L. Seol, D.-I. Moon, G. Hunter, and M. Meyyappan, ‘Nanoscale vacuum channel transistors fabricated on silicon carbide wafers’, *Nat. Electron.* 2, 405 (2019).
- [14] E. L. Murphy, and R. H. Good, Jr., ‘Thermionic emission, field emission, and the transition region’ *Phys. Rev.* 102, 1464 (1956).
- [15] R. G. Forbes, ‘Simple good approximations for the special elliptic functions in standard Fowler-Nordheim tunneling theory for a Schottky-Nordheim barrier’, *Appl. Phys. Lett.* 89, 113122 (2006).
- [16] K. L. Jensen, P. G. O’Shea, and D. W. Feldman, ‘Generalized electron emission model for field, thermal, and photoemission’, *Appl. Phys. Lett.* 81, 3867 (2002).
- [17] S.-D. Liang, and L. Chen, ‘Generalized Fowler-Nordheim theory of field emission of carbon nanotubes’, *Phys. Rev. Lett.* 101, 027602 (2008).
- [18] X. Wei, Y. Bando, and D. Golberg, ‘Electron emission from individual graphene nanoribbons driven by internal electric field’, *ACS Nano* 6, 705 (2012).
- [19] Y. S. Ang, S.-J. Liang, and L. K. Ang, ‘Theoretical modeling of electron emission from graphene’, *MRS Bulletin* 42, 505 (2017).
- [20] G. Eda, H. E. Unalan, N. Rupesinghe, G. A. J. Amaratunga, and M. Chhowalla, ‘Field emission from graphene based composite thin films’, *Appl. Phys. Lett.* 93, 233502 (2008).
- [21] M. Qian, T. Feng, H. Ding, L. Lin, H. Li, Y. Chen, and Z. Sun, ‘Electron field emission from screen-printed graphene films’, *Nanotechnology* 20, 425702 (2009).
- [22] Z.-S. Wu, S. Pei, W. Ren, D. Tang, L. Gao, B. Liu, F. Li, C. Liu, and H.-M. Cheng, ‘Field emission of single-layer graphene films prepared by electrophoretic deposition’, *Adv. Mater.* 21, 1756 (2009).
- [23] Z. Xiao, J. She, S. Deng, Z. Tang, Z. Li, J. Lu, and N. Xu, ‘Field electron emission characteristics and physical mechanism of individual single-layer graphene’, *ACS Nano* 4, 6332 (2010).
- [24] H. Yamaguchi et al., ‘Field emission from atomically thin edges of reduced graphene oxide’, *ACS Nano* 5, 4945 (2011).
- [25] Q. Ma et al, ‘Tuning ultrafast electron thermalization pathways in a van der Waals heterostructure’, *Nat. Phys.* 12, 455 (2016).
- [26] C.-K. Huang, Y. Ou, Y. Bie, Q. Zhao, and D. Yu, ‘Well-aligned graphene arrays for field emission displays’, *Appl. Phys. Lett.* 98, 263104 (2011).
- [27] D. Ye, S. Moussa, J. D. Ferguson, A. A. Baski, and M. S. El-Shall, ‘Highly efficient electron field emission from graphene oxide sheets supported by nickel nanotip arrays’, *Nano Lett.* 12, 1265 (2012).
- [28] G. Wu, X. Wei, Z. Zhang, Q. Chen, and L. Peng, ‘A graphene-based vacuum transistor with a high ON/OFF current ratio’, *Adv. Func. Mater.* 25, 5972 (2015).
- [29] G. Wu, X. Wei, S. Gao, Q. Chen, and L. Peng, ‘Tunable graphene micro-emitters with fast temporal response and controllable electron emission’, *Nature Commun.* 7, 11513 (2016).
- [30] J. Xu et al, ‘Field emission of wet transferred suspended graphene fabricated on interdigitated electrodes’, *ACS Appl. Mater. Interfaces* 8, 3295 (2016).
- [31] X. Wei, Q. Chen, and L. Peng, ‘Electron emission from two-dimensional crystal with atomic thickness’, *AIP Adv.* 3, 042130 (2013).
- [32] S. Sun, L. K. Ang, D. Shiffler, and J. W. Luginsland, ‘Klein tunnelling model of low energy electron field emission from single-layer graphene sheet’, *Appl. Phys. Lett.* 99, 013112 (2011).
- [33] W. Wang, X. Qin, N. Xu, and Z. Li, ‘Field electron emission characteristic of graphene’, *J. Appl. Phys.* 109, 044304 (2011).
- [34] D. Jena, ‘Tunneling Transistors Based on Graphene and 2-D Crystals’, *Proc. IEEE* 101, 1585 (2013).
- [35] A. A. Burkov, M. D. Hook, and L. Balents, ‘Topological nodal semimetals’, *Phys. Rev. B* 84, 235126 (2011).
- [36] M. Moore, P. Surowka, V. Juricic, and B. Roy, ‘Shear viscosity as a probe of nodal topology’, *arXiv:1912.07611v1* (2019).
- [37] B. Roy and M. S. Foster, ‘Quantum Multicriticality near the Dirac-Semimetal to Band-Insulator Critical Point in Two Dimensions: A Controlled Ascent from One Dimension’, *Phys. Rev. X* 8, 011049 (2018).
- [38] C. Fang, H. Weng, X. Dai, and Z. Fang, ‘Topological nodal line semimetals’, *Chinese Phys. B* 25 117106 (2016).
- [39] J. Wang, Y. Liu, K.-H. Jin, X. Sui, L. Zhang, W. Duan, F. Liu, and B. Huang, ‘Pseudo Dirac nodal sphere semimetal’, *Phys. Rev. B* 98, 201112(R) (2018).
- [40] J. Hu, S.-Y. Xu, N. Ni, and Z. Mao, ‘Transport of Topological Semimetals’, *Annu. Rev. Mater. Res.* 49, 207 (2019).
- [41] H.-P. Sun, and H.-Z. Lu, ‘Quantum Transport in Topological Semimetals under Magnetic Fields’, *Front. Phys.* 12, 127201 (2017); H.-P. Sun, and H.-Z. Lu, ‘Quantum Transport in Topological Semimetals under Magnetic Fields (II)’, *Front. Phys.* 14, 33405 (2019).
- [42] C. J. Tabert, J. P. Carbotte, and E. J. Nicol, ‘Optical and transport properties in three-dimensional Dirac and Weyl semimetals’, *Phys. Rev. B* 93, 085426 (2016); J. P. Carbotte, ‘Optical response of a line node semimetal’, *J. Phys.: Condens. Matter* 29 045301 (2017).
- [43] C. H. Lee, X. Zhang, and B. Guan, ‘Negative differential resistance and characteristic nonlinear electromagnetic response of a Topological Insulator’, *Scientific Reports* 5(1), 1-13 (2015).
- [44] C. H. Lee, H. H. Yap, T. Tai, G. Xu, X. Zhang, and J. Gong, ‘Enhanced higher harmonic generation from nodal topology’, *arXiv:1906.11806* (2019).
- [45] S. Ahn, E. J. Mele, and H. Min, ‘Electrodynamics on Fermi Cyclides in Nodal Line Semimetals’, *Phys. Rev. Lett.* 119, 147402 (2017).

- [46] C. M. Wang, H.-Z. Lu, and S.-Q. Shen, ‘Anomalous Phase Shift of Quantum Oscillations in 3D Topological Semimetals’, *Phys. Rev. Lett.* 117, 077201 (2016).
- [47] C. Li, C. M. Wang, B. Wan, X. Wan, H.-Z. Lu, and X. C. Xie, ‘Rules for Phase Shifts of Quantum Oscillations in Topological Nodal-Line Semimetals’, *Phys. Rev. Lett.* 120, 146602 (2018).
- [48] B. Roy, R.-J. Slager, and V. Juricic, ‘Global Phase Diagram of a Dirty Weyl Liquid and Emergent Superuniversality’, *Phys. Rev. X* 8, 031076 (2018).
- [49] S. Sur, and B. Roy, ‘Unifying Interacting Nodal Semimetals: A New Route to Strong Coupling’, *Phys. Rev. Lett.* 123, 207601 (2019).
- [50] C. H. Lee, W. W. Ho, B. Yang, J. Gong, and Z. Papić, ‘Floquet mechanism for non-Abelian fractional quantum hall states’, *Phys. Rev. Lett.* 121, 237401 (2018).
- [51] P. Zhang, A. Valfells, L. K. Ang, J. W. Luginsland, and Y. Y. Lau, ‘100 years of the physics of diodes’, *Appl. Phys. Rev.* 4, 011304 (2017).
- [52] S. Zhou, K. Chen, M. T. Cole, Z. Li, J. Chen, C. Li, and Q. Dai, ‘Ultrafast Field-Emission Electron Sources Based on Nanomaterials’, *Adv. Mater.* 31, 1805845 (2019).
- [53] S.-J. Liang, B. Cheng, X. Cui, and F. Miao, ‘Van der Waals Heterostructures for HighPerformance Device Applications: Challenges and Opportunities’, *Adv. Mater.* 1903800 (2019).
- [54] A. Allain, J. Kang, K. Banerjee, and A. Kis, ‘Electrical contacts of two-dimensional semiconductors’, *Nature Mater.* 14, 1195 (2015).
- [55] Y. Xu et al, ‘Contacts between two- and three-dimensional materials: Ohmic, Schottky, and p - n heterojunctions’, *ACS Nano* 10, 4895 (2016).
- [56] S. V. Meshkov, ‘Tunneling of electrons from a two-dimensional channel into the bulk’, *Sov. Phys. JETP* 64, 1337 (1986).
- [57] K. J. Russell, F. Capasso, V. Narayanamurti, H. Lu, J. M. O. Zide, and A. C. Gossard, ‘Scattering-assisted tunneling: Energy dependence, magnetic field dependence, and use as an external probe of two-dimensional transport’, *Phys. Rev. B* 82, 115322 (2010).
- [58] H. Zhu, J. Wang, Z. Gong, Y. D. Kim, J. Hone, and X.-Y. Zhu, ‘Interfacial charge transfer circumventing momentum mismatch at two-dimensional van der Waals heterojunctions’, *Nano Lett.* 17, 3591 (2017).
- [59] L. Britnell et al, ‘Resonant tunnelling and negative differential conductance in graphene transistors’, *Nat. Commun.* 4, 1794 (2013).
- [60] L. Britnell et al, ‘Field-Effect Tunneling Transistor Based on Vertical Graphene Heterostructures’, *Science* 335, 947 (2012).
- [61] T. Roy, L. Liu, S. de la Barrera, B. Chakrabarti, Z. R. Hesabi, C. A. Joiner, R. M. Feenstra, G. Gu, and E. M. Vogel, ‘Tunneling characteriss in chemical vapor deposited graphene-hexagonal boron nitride-graphene junctions’, *Appl. Phys. Lett.* 104, 123506 (2014).
- [62] Y. S. Ang, Y. Chen, C. Tan, and L. K. Ang, ‘Generalized High-Energy Thermionic Electron Injection at Graphene Interface’, *Phys. Rev. Appl.* 12, 014057 (2019).
- [63] E. E. Vdovin et al, ‘Phonon-Assisted Resonant Tunneling of Electrons in GrapheneBoron Nitride Transistors’, *Phys. Rev. Lett.* 116, 186603 (2016).
- [64] D. Ghazaryan et al, ‘Magnon-assisted tunnelling in van der Waals heterostructures based on CrBr_3 ’, *Nat. Electron.* 1, 344 (2018).
- [65] U. Chandni, K. Watanabe, T. Taniguchi, and J. P. Eisenstein, ‘Signatures of Phonon and Defect-Assisted Tunneling in Planar Metal-Hexagonal Boron Nitride-Graphene Junctions’, *Nano Lett.* 16, 7982 (2016).
- [66] See Supplemental Material for a discussion of $D(\varepsilon_{\parallel}, F)$, the explicit forms of v_0 and t_0 , and the detailed derivations of \mathcal{J}_{uni} , \mathcal{J}_{NP} , \mathcal{J}_{QCP} , \mathcal{J}_{NL} , \mathcal{J}_{Gr} and \mathcal{J}_{FB} .
- [67] J. Kim et al, ‘Observation of tunable band gap and anisotropic Dirac semimetal state in black phosphorus’, *Science* 349, 723 (2015); S. W. Jung et al, ‘Black phosphorus as a bipolar pseudospin semiconductor’, *Nat. Mater.* 19, 227 (2020).
- [68] H. Chen, S. Zhang, W. Jiang, C. Zhang, H. Guo, Z. Liu, Z. Wang, F. Liu, and X. Niu, ‘Prediction of two-dimensional nodal-line semimetals in a carbon nitride covalent network’, *J. Mater. Chem. A* 6, 11252 (2018).
- [69] F. Xia, V. Perebeinos, Y.-M. Lin, Y. Wu, and P. Avouris, ‘The origins and limits of metalgraphene junction resistance’, *Nat. Nanotechnol.* 6, 179 (2011).
- [70] Sinha, and J.-U. Lee, ‘Ideal graphene/silicon Schottky junction Diodes’, *Nano Lett.* 14, 4660 (2014).
- [71] M. Massicotte et al, ‘Photo-thermionic effect in vertical graphene heterostructures’, *Nature Commun.* 7, 12174 (2016).
- [72] Y.-J. Yu, Y. Zhao, S. Ryu, L. E. Brus, K. S. Kim, and P. Kim, ‘Tuning the graphene work function by electric field effect’, *Nano Lett.* 9, 3430 (2009).
- [73] S. Wang et al, ‘Efficient Carrier-to-Exciton Conversion in Field Emission Tunnel Diodes Based on MIS-Type van der Waals Heterostack’, *Nano Lett.* 8, 5156 (2017).
- [74] A. Mielke, ‘Ferromagnetic ground states for the Hubbard model on line graphs’, *J. Phys. A: Math. Gen.* 24, L73 (1991).
- [75] E. H. Lieb, ‘Two Theorems on the Hubbard Model’, *Phys. Rev. Lett.* 62, 1201 (1989).
- [76] A. Raoux, M. Morigi, J.-N. Fuchs, F. Piechon, and G. Montambaux, ‘From Dia- to Paramagnetic Orbital Susceptibility of Massless Fermions’, *Phys. Rev.* 111, 026402 (2011).
- [77] C. H. Lee, M. Claassen, and R. Thomale, ‘Band structure engineering of ideal fractional Chern insulators’, *Phys. Rev. B* 96, 165150 (2017).
- [78] F. Castro de Lima, G. J. Ferreira, and R. H. Miwa, ‘Topological flat band, Dirac fermions and quantum spin Hall phase in 2D Archimedean lattices’, *Phys. Chem. Chem. Phys.* 21, 22344 (2019).
- [79] R. Bi, Z. Yan, L. Lu, and Z. Wang, ‘Nodal-knot semimetals’, *Phys. Rev. B* 96, 201305(R) (2017).
- [80] M. Ezawa, ‘Topological semimetals carrying arbitrary Hopf numbers: Fermi surface topologies of a Hopf link, Solomon’s knot, trefoil knot, and other linked nodal varieties’, *Phys. Rev. B* 96, 041202 (2017).
- [81] C. H. Lee, T. Hofmann, T. Helbig, Y. Liu, X. Zhang, M. Greiter, and R. Thomale, ‘Imaging nodal knots in momentum space through topoelectrical circuits’, arXiv:1904.10183 (2019).
- [82] L. Li, C. H. Lee, and J. Gong, ‘Emergence and full 3D-imaging of nodal boundary Seifert surfaces in 4D topological matter’, *Commun Phys* 2, 135 (2019), <https://doi.org/10.1038/s42005-019-0235-4>.
- [83] B. Bode, and M. R. Dennis, ‘Constructing a polynomial whose nodal set is any prescribed knot or link’, *Journal of Knot Theory and Its Ramifications* 28, 1850082 (2019).
- [84] S. Roche et al, ‘Graphene spintronics: the European

- Flagship perspective', *2D Mater.* 2, 030202 (2015).
- [85] Y. S. Ang, S. A. Yang, C. Zhang, Z. Ma, and L. K. Ang, 'Valleytronics in merging Dirac cones: All-electric-controlled valley filter, valve, and universal reversible logic gate', *Phys. Rev. B* 96, 245410 (2017).
- [86] L. Sun, Y. Zhang, G. Hwang, J. Jiang, D. Kim, Y. A. Eshete, R. Zhao, and H. Yang, 'Synaptic Computation Enabled by Joule Heating of Single-Layered Semiconductors for Sound Localization', *Nano Lett.* 18, 3229 (2018).
- [87] C. Heide, M. Hauck, T. Higuchi, J. Ristein, L. Ley, H. B. Weber, and P. Hommelhoff, 'Attosecond-fast internal photoemission', *Nat. Photonics*, <https://doi.org/10.1038/s41566-019-0580-6> (2020).
- [88] F. Rezaeifar, R. Ahsan, Q. Lin, H. U. Chae, and R. Kapadia, 'Hot-electron emission processes in waveguide-integrated graphene', *Nat. Photon.* 13, 843 (2019).
- [89] C. Li et al, 'Extreme nonlinear strong-field photoemission from carbon nanotubes', *Nat. Commun.* 10, 4891 (2019).